ORGANOMETALLICS
Article
Cite This: Organometallics 2020, 39, 93−104
pubs.acs.org/Organometallics

Assembled Multinuclear Ruthenium(II)−NNNN Complexes: Synthesis, Catalytic Properties, and DFT Calculations

Tingting Liu,[†,‡,§] Kaikai Wu,[†] Liandi Wang,[†] Hongjun Fan,*[,†,∥] Yong-Gui Zhou,*[,†] and Zhengkun Yu*[,†,⊥]

[†]Dalian Institute of Chemical Physics, Chinese Academy of Sciences, 457 Zhongshan Road, Dalian, Liaoning 116023, PR China
[‡]University of Chinese Academy of Sciences, Beijing 100049, PR China
[§]Institute of Chemistry, Henan Academy of Sciences, Zhengzhou 450002, PR China
[∥]State Key Laboratory of Molecular Reaction Dynamics, Dalian Institute of Chemical Physics, Chinese Academy of Sciences, 457 Zhongshan Road, Dalian 116023, PR China
[⊥]State Key Laboratory of Organometallic Chemistry, Shanghai Institute of Organic Chemistry, Chinese Academy of Sciences, 354 Fenglin Road, Shanghai 200032, PR China

Supporting Information

ABSTRACT: Using a coordinatively unsaturated 16-electron mononuclear ruthenium(II)-pyrazolyl-imidazolyl-pyridine complex [Ru(II)−NNN] as the building block and oligopyridines as the polydentate ligands, pincer-type tri- and hexanuclear ruthenium(II) complexes $[Ru(II)−NNNN]_n$ were efficiently assembled. These complexes were characterized by elemental analyses, NMR, IR, and MALDI-TOF mass spectroscopies. In refluxing 2-propanol, the multinuclear ruthenium(II)−NNNN complexes exhibited exceptionally high catalytic activity for the transfer hydrogenation of ketones at very low concentrations and reached turnover frequencies (TOFs) up to 7.1×10^6 h^{-1}, featuring a remarkable cooperative effect from the multiple Ru(II)−NNNN functionalities. DFT calculations have revealed the origin of the high catalytic activities of these Ru(II)−NNNN complexes.

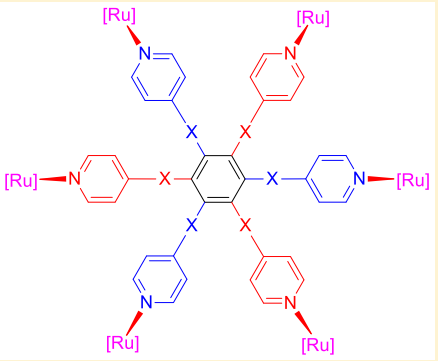

INTRODUCTION

In homogeneous catalysis and organic synthesis, construction of an efficient catalyst system has been a challenging task.[1] Multinuclear complex catalysts have recently been paid much attention because they are usually expected to exhibit different reactivity in comparison to that of the corresponding mononuclear complexes due to the possible electronic interactions between the metal centers and cooperative activation of the substrates.[2] In this regard, noncovalent interactions,[3] such as van der Waals, $\pi-\pi$ stacking, metal−ligand interactions, dipole−dipole interaction, hydrogen bonding, and so on, have been used for the construction of multinuclear structures inspired by many functional biological systems, which results in fascinating catalytic,[4] electrochemical,[5] photophysical,[6] magnetic,[7] and host−guest[8] properties. Coordination-driven assembly evolved into a useful methodology to access multinuclear structures due to its highly directional and predictable feature and specific stoichiometry.[9] Stang et al. established the general principle for the construction of macrocycles using ditopic subunits.[10] Anderson and co-workers used oligopyridines to assemble with small template molecules for the direct synthesis of macrocyclic zinc-porphyrin nanorings.[11] To date, many multinuclear complexes have been constructed by assembly of monometallic building blocks and a polydentate ligand,[12] among which Bera and co-workers developed a diruthenium Ru(II)−NNNN complex incorporating a naphthyridine−diimine ligand as an efficient catalyst for the acceptorless dehydrogenation of alcohols,[12b] and they also synthesized a Ru(II)−CNNO complex catalyst bearing naphthyridine-functionalized *N*-heterocyclic carbene (NHC) ligands for the dehydrogenative coupling reactions between alcohols and amines, exhibiting both metal−metal and metal−ligand cooperation.[12c] Although the preparation methods and stoichiometric reactivity of multinuclear complexes have been extensively investigated, less attention has been paid to their catalytic activities.[13]

Catalytic transfer hydrogenation (TH) reaction has been considered as a concise method for the reduction of ketones to the corresponding alcohols.[14] Mononuclear ruthenium(II) complexes have usually been applied as the catalysts for such TH reactions,[15−18] but multinuclear ruthenium(II) complexes have rarely been studied in this area. During the ongoing investigation of pincer-type Ru(II)−NNN complex catalysts for TH reaction,[19] we established several highly active pincer-type diruthenium(II) complex catalysts,[20] among which complex **A**[20c] was assembled by means of coordinatively unsaturated 16-electron mononuclear ruthenium(II)-pyrazolyl-

Received: October 9, 2019
Published: December 19, 2019

DOI: 10.1021/acs.organomet.9b00669
Organometallics 2020, 39, 93−104

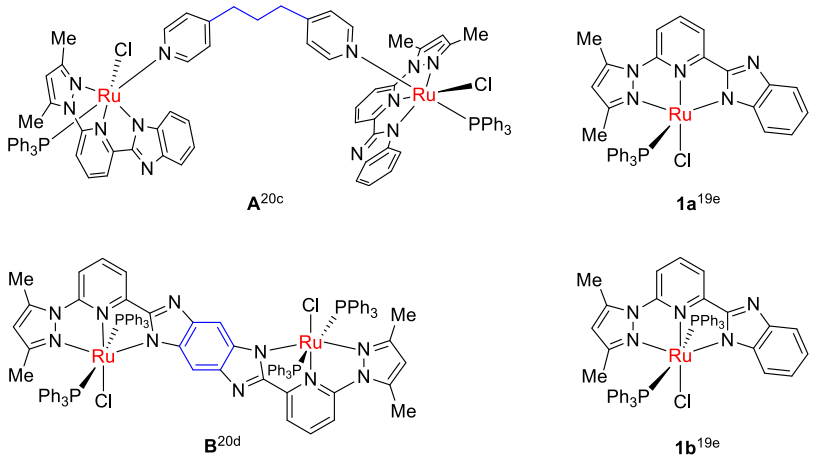

Figure 1. Our previous work on dinuclear Ru(II)−NNNN complex catalysts.[19e,20c,d]

imidazolyl-pyridine complex **1a** and 4,4′-$(CH_2)_3$-linked bipyridine and complex **B**[20d] was constructed by using a π-linker-supported bis(pyrazolyl-imidazolyl-pyridine) ligand (Figure 1). As compared with corresponding mononuclear pincer-type Ru(II)−NNN complexes **1a** and **1b**,[19e] diruthenium(II) complexes **A** and **B** exhibit much higher catalytic activities for the TH reactions of ketones, demonstrating a remarkable cooperative effect from the diruthenium metal centers. Complex **A** is bestowed with the most flexible molecular structure in which the two metal centers may cooperatively interact in the confined microenvironment and thus enhance the catalytic activity of the complex. The high catalytic activity of complex **B** is presumably attributed to its good stability and the possible cooperativity of the two coexisting metal centers coordinated by the coplanar NNN-heteroaryl-NNN ligand.

Due to the easy manipulation and high efficiency related to the assembly strategy for the construction of a multinuclear complex,[9−13] we envisioned that coordinatively unsaturated 16-electron pincer-type Ru(II)−NNN complex **1a**,[19e] as a mononuclear complex building block, might be utilized to assemble multinuclear Ru(II)−NNNN complexes in the presence of polydentate nitrogen-containing ligands. Herein, we disclose the synthesis, characterization, and catalytic properties of the tri- and hexanuclear ruthenium(II)−NNNN complexes assembled by using a 16-electron mononuclear complex building block and polydentate oligopyridine ligands (Scheme 1). DFT calculations were also conducted to rationalize the exceptionally high catalytic activities of these Ru(II)−NNNN complexes at very low concentrations.

Scheme 1. Strategy To Assemble Multinuclear Ru(II)−NNNN Complexes

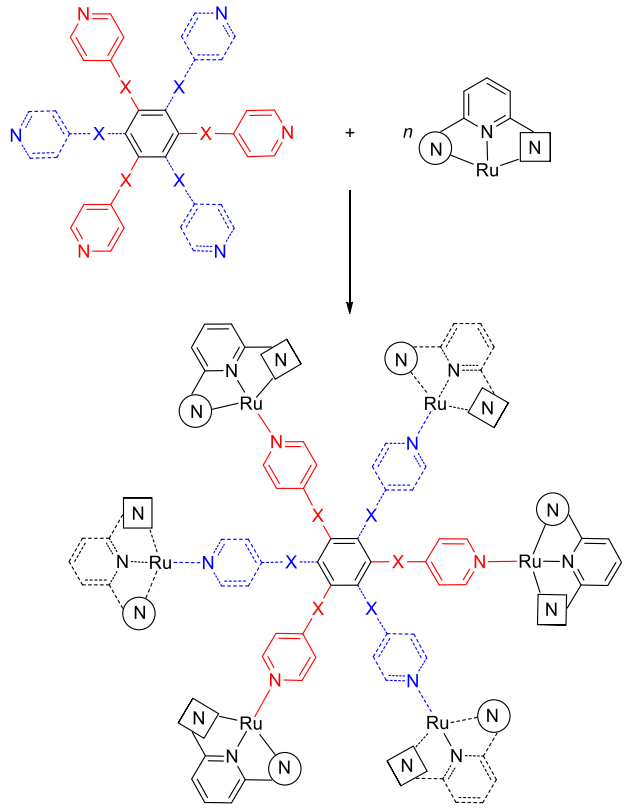

RESULTS AND DISCUSSION

Synthesis of Multinuclear Ru(II)−NNNN Pincer Complexes. Oligopyridines 1,3,5-tri(pyridin-4-yl)benzene (**2a**)[21a] and 4,4′-(5′-(4-(pyridin-4-yl)phenyl)-[1,1′:3′,1″-terphenyl]-4,4″-diyl)dipyridine (**2b**)[21b] were prepared and applied to the synthesis of trinuclear Ru(II)−NNNN pincer complexes **3** and **4**, respectively, from their reactions with the mononuclear Ru(II)−NNN complex **1a** by means of the assembly strategy as shown in Scheme 1. At ambient temperature, treatment of complex **1a** and oligopyridine **2a** in a 3:1 molar ratio in the mixed solvent of CH_2Cl_2/MeOH (v/v, 5/1) afforded complex **3** in 94% yield (Scheme 2). In a similar manner, the reaction of ligand **2b** with **1a** efficiently formed complex **4** (91%). To evaluate the steric and electronic impacts of the oligopyridine ligands on the catalytic activity of the resultant multimetallic complexes, hexanuclear Ru(II)−NNNN pincer complexes **6** and **7** were also prepared (91−92%) from the reactions of complex **1a** and oligopyridine ligands **5a** and **5b**[21c,d] in a 6:1 molar ratio (Scheme 3). In ligands **2** and **5**, the linkers (spacers) varied from terphenyl to ethynyl-bridged terphenyl. In order to make a comparison, a relevant mononuclear Ru(II)−NNNN pincer complex, that is, complex **9**, was also synthesized (92%) from the 1:1 molar ratio reaction of complex **1a** with 4-phenylpyridine (**8**):

DOI: 10.1021/acs.organomet.9b00669
Organometallics 2020, 39, 93−104

Scheme 2. Synthesis of Trinuclear [Ru(II)−NNNN]$_3$ Complexes

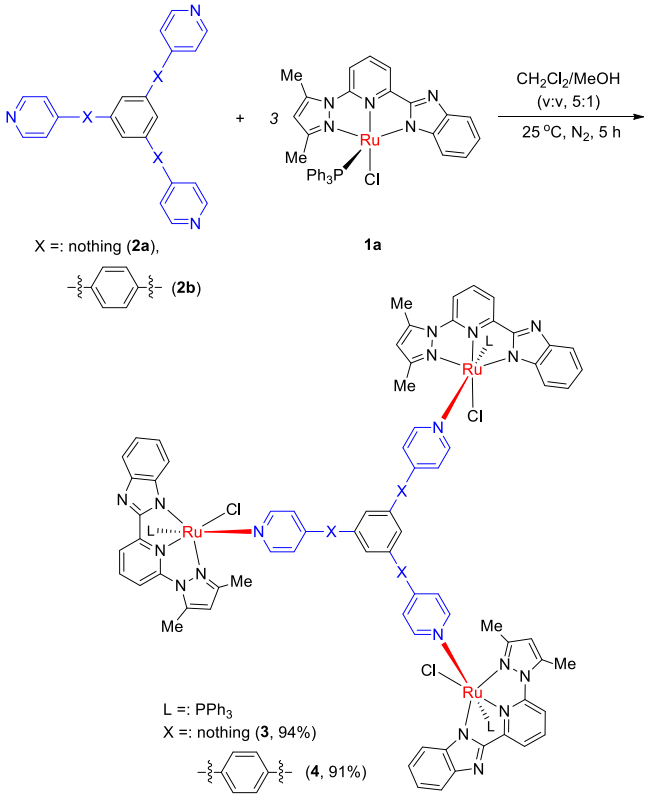

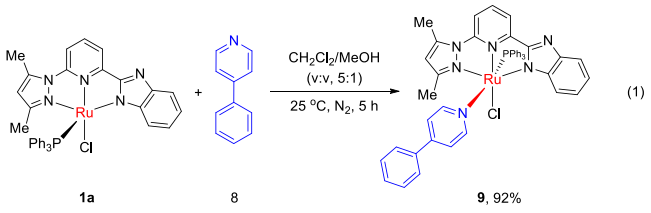

Scheme 3. Synthesis of Hexanuclear [Ru(II)−NNNN]$_6$ Complexes

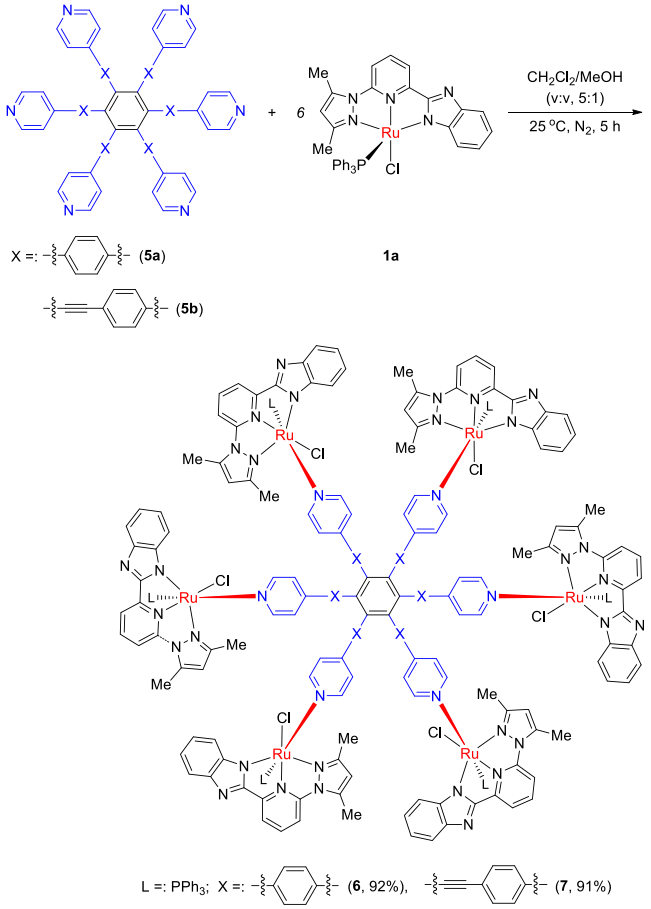

Characterization of the Complexes. Complexes **3**, **4**, **6**, **7**, and **9** were fully characterized by NMR and FT-IR spectroscopies, elemental analysis, and MALDI-TOF mass spectrometry. The NMR analyses are consistent with their compositions. The ^{1}H NMR spectrum of complex **3** reveals two doublets at 8.71 and 8.00 ppm for the 4-pyridyl moiety of ligand **2a** and a singlet at 8.27 ppm for the 1,3,5-phenyl core, respectively. The resonance signal of the three pyrazolyl-CH protons appears at 6.38 ppm as a singlet, suggesting occurrence of Ru−N coordination between ligand **2a** and the Ru(II)−NNN building block, that is, mononuclear Ru(II)−NNN complex **1a**, which led to complex **3**. Similarly, the proton resonance signals of the 4-pyridyl moiety appear at 8.69 and 7.81 ppm as two doublets, and that of the 1,3,5-triphenyl-substituted benzene core is shown at 8.09 ppm as a singlet, revealing the existence of ligand **2b** in trinuclear complex **4**. The ^{1}H NMR spectrum of complex **6** exhibits two doublets at 8.42 and 7.57 ppm, respectively, corresponding to the proton resonances of the 4-pyridyl moieties of ligand **5a**, and the resonance signal of the six pyrazolyl-CH protons appears at 6.37 ppm as a singlet. These spectral features have suggested the occurrence of Ru−N coordination between mononuclear complex **1a** and ligand **5a** in complex **6**. Two doublets appear at 8.57 and 7.20 ppm for the resonance signals of the 4-pyridyl moieties of ligand **5b** in the ^{1}H NMR spectrum of complex **7**, and the resonance signals at 93.9 and 87.0 ppm in the ^{13}C{^{1}H} NMR spectrum reveal existence of the ethynyl moiety, suggesting the presence of ligand **5b** in complex **7**. The ^{31}P NMR signals are shown at 33.5, 33.5, 33.5, 33.0, and 33.5 ppm for complexes **3**, **4**, **6**, **7**, and **9** in the ^{31}P{^{1}H} NMR spectra, respectively, implicating a similar coordination pattern around the Ru(II) metal centers in these Ru(II)−NNNN complexes. In comparison to the ^{31}P{^{1}H} NMR spectrum of complex **1a** (δ(^{31}P) = 33.8 ppm),[19e] it is clear that the ^{31}P resonance signals of complexes **3**, **4**, **6**, **7**, and **9** are shifted 0.3−0.8 ppm upfield, suggesting that the coordinatively unsaturated metal center in Ru(II)−NNN complex **1a** is more electronically positive than those in the coordinatively saturated Ru(II)−NNNN complexes. The compositions of complexes **3**, **4**, **6**, and **7** were also analyzed by MALDI-TOF mass spectrometry. The molecular ion peaks [**3** + H]$^+$, [**4** + H]$^+$, [**6** + H]$^+$, and [**7** + H]$^+$ were not observed in the mass spectra, while those peaks corresponding to the fragments [**1a** + H]$^+$, [**2** + H]$^+$, and [**5** + H]$^+$ were detected, respectively. It is noteworthy that the fragment of mononuclear building block complex **1a**, that is, [**1a** + H]$^+$, was found in the mass spectra of all complexes **3**, **4**, **6**, and **7**, coalesced by the protonated ligand fragments, which has suggested the possible compositions of the complexes. Theoretical stimulation of the mass spectra is consistent with the experimental results (see the Supporting Information for details).

Comparison of the Catalytic Activities of Complexes 3, 4, 6, 7, and 9. Next, the TH reactions of selected ketones

DOI: 10.1021/acs.organomet.9b00669
Organometallics 2020, 39, 93−104

were performed to compare the catalytic activities of complexes **3**, **4**, **6**, **7**, and **9** (Table 1). Under the typical conditions for a TH reaction,[19] acetophenone was reduced to 1-phenylethanol in refluxing 2-propanol. With a loading of 0.025 mol % Ru for a complex catalyst, the TH reaction proceeded smoothly, furnishing the target alcohol product in 96−98% yields over a period of 1−2 min by using complexes **3**, **4**, and **6** (Table 1, entry 1), exhibiting a positive cooperative effect from the multiple Ru(II)−NNNN functionalities. It is noteworthy that mononuclear Ru(II)−NNN complex **1a** could only be applied as the catalyst for the same reactions at $a \geq$ 0.05 mol % Ru loading.[19e] Complex **7** showed a much lower catalytic activity than complexes **3**, **4**, **6**, and **9**, rendering formation of 1-phenylethanol in 90% yields over a period of 30 min, which is presumably attributed to the introduction of an ethynyl linker (spacer) into the ligand that disfavors the electron transfer in a multimetallic complex molecule.[22] Under the same conditions, bimetallic complex **B** can be applied as the catalyst for the TH reaction of acetophenone at a minimum Ru loading of 0.05 mol %, achieving 98% yield and a TOF value of 1.5×10^5 h^{-1} within 20 min.[20d] The present results have revealed that complexes **3**, **4**, and **6** are much more catalytically active than bimetallic complex **B** at a lower ruthenium loading. Complexes **3**, **4**, and **6** could all efficiently catalyze the TH reaction of 2′-chloroacetophenone to completion within 1/6 min. Complex **3** achieved the highest TOF value 7.1×10^6 h^{-1} by using a catalyst loading as low as 0.008 mol % Ru; both complexes **4** and **6** could be used as the catalysts with a loading as low as 0.0125 mol % Ru (Table 1, entry 2). However, a minimum loading of 0.025 mol % Ru was required for complexes **7** and **9**. Both 3′- and 4′-chloroacetophenones efficiently underwent the TH reactions in the presence of complex catalysts **3**, **4**, and **6**, respectively, whereas complex **9** required a longer time for completing the reactions at the same ruthenium loadings (Table 1, entries 3 and 4), revealing the lower catalytic activity of complex **9**. It seems that the ethynyl linker in complex **7** remarkably diminished its catalytic activity for the same reactions. Complex **3** catalyzed the TH reaction of sterically hindered 2′-methylacetophenone to reach 98% yield within 5 min, and complex **6** promoted the same reaction to give the product in 97% yield over a period of 30 min, while complexes **4**, **7**, and **9** catalyzed the same reaction to form the target product in 45−62% yields within 30 min (Table 1, entry 5). Overall, complex **3** exhibited the highest catalytic activity in most of the TH reactions of the selected acetophenones as shown in Table 1. Oligopyridine ligand **2a** may bestow assembled pincer-type triruthenium(II)−NNNN complex **3** with the most compatible steric and electronic impacts on the ruthenium metal centers, which thus enhances its catalytic activity for the transfer hydrogenation of ketones. In comparison to those known dinuclear pincer-type Ru(II)−NNNN complexes,[20] tri- and hexanuclear complexes **3**, **4**, and **6** could exhibit much higher catalytic activity in the TH reactions of acetophenones.

The reaction kinetics was studied by the TH reaction of 4′-chloroacetophenone to understand the catalytic activity differences between complexes **3**, **4**, **6**, **7**, and **9** (Figure 2). It is clear that complexes **3**, **4**, and **6** exhibited much higher catalytic activities than those of complexes **7** and **9** with the catalytic activity order **3** ≥ **4** > **6** > **9** > **7** under the stated conditions. The curves for the calculated turnover frequencies against the concentrations of 4′-chloroacetophenone for the five complex catalysts fall on top of each other, which implicates that catalyst deactivation is not a factor in this TH reaction, and the catalytic activity differences were caused by

Table 1. Comparison of the Catalytic Activities of Complexes 3, 4, 6, 7, and 9[a]

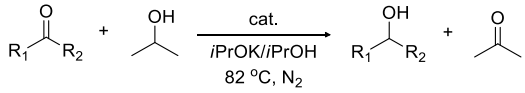

Entry	Ketone	Cat.	Time (min)	Yield[b] (%)	TOF[c] (h^{-1})
1	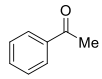	**3**	1	96	1.6×10^6
		4	1	98	2.4×10^6
		6	2	96	5.6×10^5
		7	30	90	6.7×10^5
		9	1	97	1.1×10^6
2	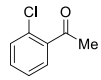	**3**[d]	2	97	7.1×10^6
		4[e]	20	96	1.2×10^6
		6[e]	1	97	2.9×10^6
		7	1	99	2.0×10^6
		9	1	99	8.1×10^5
3	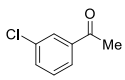	**3**[e]	2	98	9.6×10^5
		4[e]	2	97	1.3×10^6
		6	1	99	2.6×10^6
		7	2	96	6.7×10^5
		9	1	97	9.0×10^5
4	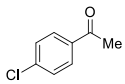	**3**[d]	2	97	5.2×10^6
		4[e]	1	99	3.4×10^6
		6	1	98	1.3×10^6
		7	10	96	7.0×10^5
		9	5	97	6.8×10^5
5	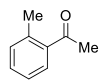	**3**	5	98	7.4×10^5
		4	30	47	-
		6	30	97	1.0×10^5
		7	30	45	-
		9	30	62	-

[a]Conditions: ketone, 2.0 mmol (0.1 M in 20 mL *i*PrOH); 0.025 mol % Ru (ketone/*i*PrOK/Ru = 4000:20:1); 0.1 MPa N_2, 82 °C. [b]Determined by GC analysis. [c]Turnover frequency (moles of ketone converted per mole of Ru per hour) at 50% conversion of the ketone substrate. [d]Using 0.008 mol % Ru. [e]Using 0.0125 mol % Ru.

DOI: 10.1021/acs.organomet.9b00669
Organometallics 2020, 39, 93−104

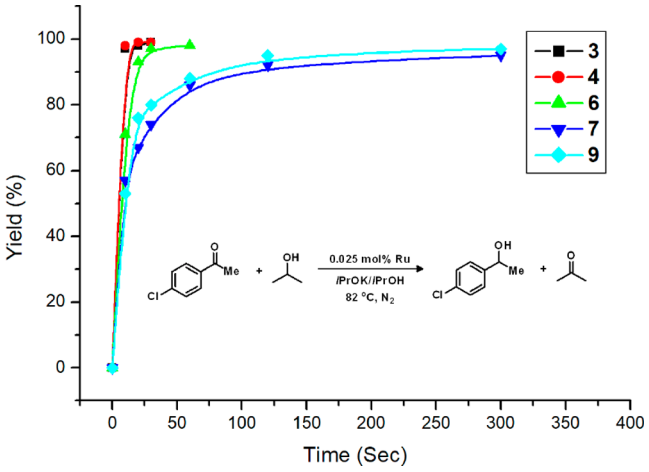

Figure 2. Representative reaction kinetics profiles.

the inherent catalyst rates of the complex catalysts[23c] (Figure 3).

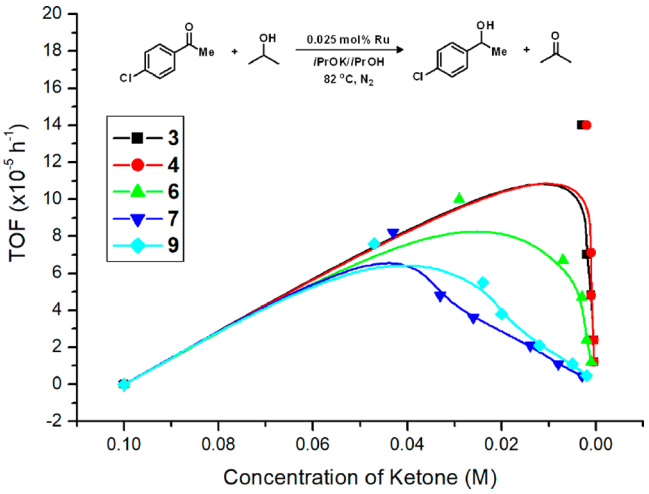

Figure 3. Correlation of TOFs and concentrations of the ketone.

Transfer Hydrogenation of Ketones Catalyzed by Complexes 3, 4, and 6. Then, the TH reactions of various ketones were explored by using complexes **3**, **4**, and **6** as the catalysts. With a 0.025 mol % Ru loading, complexes **3**, **4**, and **6** efficiently catalyzed the TH reaction of acetophenone in refluxing 2-propanol, forming the target alcohol product in 96−98% yield within 1−2 min (Table 2, entry 1). However, propiophenone required a higher catalyst loading, i.e., 0.1 mol % Ru, to complete the reaction (Table 2, entry 2). For the reduction of methyl-substituted acetophenones, a higher catalyst loading (0.05−0.1 mol % Ru) was usually necessary for complex **4** (Table 2, entries 3−5). A smaller amount of complex catalyst **3** but a higher loading of complex **6** was provided for the TH reaction of 3′-methoxyacetophenone (Table 2, entry 6), reaching TOFs ranging from 4.2×10^5 to 5.2×10^6 h^{-1}. The chloro and bromo substituents favored the TH reactions, and the catalyst loading could be further reduced to 0.0125 or 0.008 mol % Ru (Table 2, entries 7−11). In the cases of 2′-chloroacetophenone and 4′-bromoacetophenone, complex **3** exhibited a very high catalytic activity with a 0.008 mol % Ru loading, reaching TOF values 7.1×10^6 h^{-1} and 5.8×10^6 h^{-1}, respectively. Baratta et al. reported the transfer hydrogenation reaction of 3′-bromoacetophenone catalyzed by a monometallic Ru(II)−CNN complex catalyst bearing an NH functionality, achieving a TOF value 3.8×10^6 h^{-1}.[23a] Our complexes **3** and **6** are unambiguously among the few known most active transition metal complex catalysts for the transfer hydrogenation of ketones to date. Fluoro- and trifluoromethyl-substituted acetophenones were also efficiently reduced to the corresponding alcohols. In the case of using complex **3** as the catalyst, the reactivity order of the ketone substrates is 2′-CF_3 > 4′-CF_3 > 3′-CF_3, while the reactivity order was altered to 4′-CF_3 > 2′-CF_3 > 3′-CF_3 by using complexes **4** and **6** as the catalysts (Table 2, entries 14−16), suggesting that the coordinating arms of the ligand may affect the interaction of the substrate with the catalytically active metal center. Both sterically hindered benzophenone and 2-acetylnaphthalene, as well as aliphatic cyclic and acyclic ketones, could also be reduced to the corresponding alcohols by variation of the reaction time and catalyst loadings (Table 2, entries 17−20).

Tentative Preparation of the Ruthenium(II)−NNNN Hydride Complexes. To probe into the reaction mechanism, the preparation of catalytically active species was attempted by reacting complex **3** with a base in refluxing 2-propanol under the TH reaction conditions. The Ru(II) hydride complexes generated from the corresponding Ru(II)−Cl complex catalyst precursors are usually considered as the catalytically active species for the transfer hydrogenation of ketones.[17b,18−20] Thus, complex **3** was reacted with *t*BuOK or *i*PrOK in 2-propanol under a nitrogen atmosphere. Unfortunately, the expected triruthenium(II) hydride complex was not successfully isolated, and no RuH species was detected in the reaction mixture by proton NMR spectral analysis. Complex **3** was also reacted with $NaBH_4$ at 0 °C under a nitrogen atmosphere or treated with HCO_2H/Et_3N or atmospheric hydrogen in isopropanol at room temperature to 50 °C; no RuH species was detected in the reaction mixtures by proton NMR spectral analysis. These results have suggested that the multinuclear Ru(II)−NNNN hydride complexes are unstable under the stated conditions as compared with those mononuclear Ru(II)−NNN hydride complexes generated from the mononuclear Cl−Ru(II)−NNN complexes.[19,20,24]

Theoretical Calculations. DFT (M06−2x[25] functional, def2-tzvp for ruthenium and cc-pVDZ for other atoms, and Gaussian16)[26] calculations were conducted to study the structures of the multinuclear Ru(II)−NNNN complexes and the possible catalytically active species in the TH reactions of ketones, and we rationalize the enhanced catalytic activity of these complexes (see the Supporting Information for details).

Coordination and Optimized Structures. First, the coordination structure of complex **3** was investigated by using its mononuclear analog, that is, the 1:1 molar ratio adduct of mononuclear Ru(II)−NNN complex **1a** and ligand **2a** (**1a**·**2a**, Scheme 4), in which ligand **2a** only contributes one pyridyl moiety to coordinate with the metal center of complex **1a** (Scheme 3). It was found that in the most stable conformation of the resultant mononuclear Ru(II)−NNNN complex **10**, the PPh_3 ligand is positioned trans to ligand **2a**, which is exactly the same as that shown in Scheme 2. The conformer with the Cl atom trans to ligand **2a**, that is, complex **10a**, is less stable by 14.1 kcal/mol than the former, and the conformer of complex **10b** with the NNN ligand of **1a** trans to ligand **2a** is less stable by 12.5 kcal/mol. A similar structure was found for complex **9**, the 1:1 molar ratio adduct of complex **1a** and

DOI: 10.1021/acs.organomet.9b00669
Organometallics 2020, 39, 93−104

Table 2. Transfer Hydrogenation of Ketones Catalyzed by Complexes 3, 4, and 6[a]

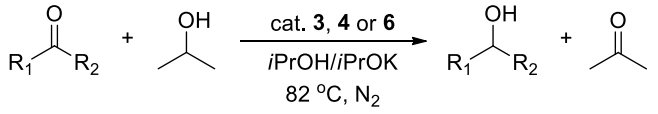

Entry	Ketone	Cat.	Time (min)	Yield[b] (%)	TOF[c] (h^{-1})
1		**3**	1	96	1.6×10^6
		4	1	98	2.4×10^6
		6	2	96	5.6×10^5
2		**3**[d]	1	99	6.0×10^5
		4[d]	10	97	3.8×10^4
		6[d]	5	98	2.9×10^4
3		**3**	5	98	7.4×10^5
		4[d]	5	98	1.2×10^5
		6	30	97	1.0×10^5
4	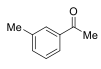	**3**	2	96	1.4×10^6
		4[e]	1	97	1.0×10^6
		6[d]	5	98	2.4×10^5
5	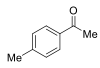	**3**	2	96	1.3×10^6
		4[d]	5	96	1.8×10^5
		6	10	96	2.2×10^5
6	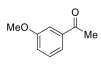	**3**[f]	2	97	5.2×10^6
		4	2	97	6.8×10^5
		6[e]	5	98	4.2×10^5
7		**3**[g]	2	97	7.1×10^6
		4[f]	20	96	1.2×10^6
		6[f]	1	97	2.9×10^6
8	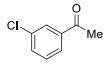	**3**[f]	2	98	9.6×10^5
		4[f]	2	97	1.3×10^6
		6	1	99	2.6×10^6
9	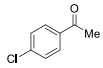	**3**	2	97	5.2×10^6
		4	1	99	3.4×10^6
		6	1	98	1.3×10^6
10	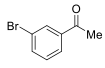	**3**[g]	30	96	2.4×10^6
		4	1	98	1.6×10^6
		6	2	99	7.6×10^5
11	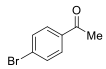	**3**[g]	10	96	5.8×10^6
		4[f]	2	98	2.7×10^6
		6[f]	5	98	1.4×10^6
12		**3**	2	97	2.1×10^6
		4[e]	2	99	4.9×10^5
		6[e]	20	97	3.6×10^5
13	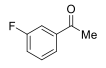	**3**[f]	1	99	5.1×10^6
		4	2	99	1.8×10^6
		6[e]	5	99	1.8×10^5
14		**3**[f]	20	97	8.6×10^5
		4	2	99	1.0×10^6
		6	20	98	3.8×10^5
15	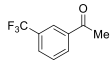	**3**	10	96	5.5×10^5
		4[e]	1	98	8.2×10^5
		6	30	96	5.5×10^4
16	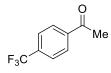	**3**	2	96	1.4×10^6
		4	1	98	7.0×10^5
		6	1	99	1.3×10^6
17	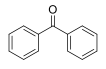	**3**	30	92	3.6×10^6
		4[f]	2	97	1.5×10^6
		6	1	97	8.3×10^5
18	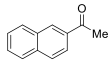	**3**	30	87	1.8×10^6
		4	2	96	2.5×10^6
		6	10	96	2.8×10^5
19		**3**	1	96	1.7×10^6
		4[e]	5	99	1.7×10^5
		6[d]	2	99	1.4×10^5
20		**3**[e]	2	98	3.6×10^5
		4[d]	1	99	4.1×10^5
		6[d]	5	98	8.1×10^4

[a]Conditions: ketone, 2.0 mmol (0.1 M in 20 mL *i*PrOH); 0.025 mol % Ru (ketone/*i*PrOK/Ru = 4000:20:1); 0.1 MPa N_2, 82 °C. [b]Determined by GC analysis. [c]Turnover frequency (moles of ketone converted per mole of Ru per hour) at 50% conversion of the ketone substrate. [d]0.1 mol % Ru. [e]0.05 mol % Ru. [f]0.0125 mol % Ru. [g]0.008 mol % Ru.

ligand 4-phenylpyridine (**8**) (eq 1). In trinuclear Ru(II)−NNNN complex **3**, ligand **2a** is situated at the molecular core, and the three PPh_3 ligands are placed at the peripheral positions of the Ru-NNN building block planes. It has been well-known that transition metal catalyzed organic transformations often occur via a ligand dissociation−substrate coordination mechanism. In our case, the PPh_3 ligand is initially dissociated to offer a coordinatively unsaturated site at

DOI: 10.1021/acs.organomet.9b00669
Organometallics 2020, 39, 93−104

Scheme 4. Coordination Structures of Adduct 1a·2a

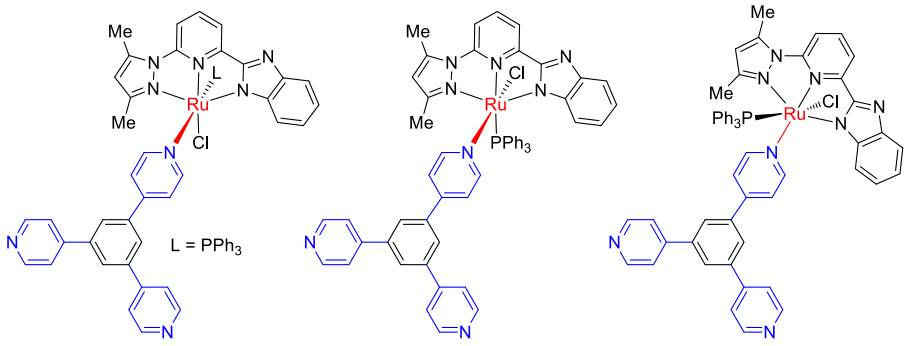

the metal center for coordination−activation of the ketone substrate in the catalytic cycle. The calculations have revealed that dissociation of the PPh_3 ligand does not obviously change the structure of the Ru metal center in complex **10**. Thus, in the subsequent calculations the PPh_3 ligand was omitted in the theoretical models. With this simplification, the structures of corresponding monohydride complex **3′** from complex **3** (Figure 4), which is supposed to be the catalytically active species for the TH reaction, and complex **3″** in which the Ru−H metal center of complex **3′** is coordinated by one molecule of the ketone substrate (simplified as acetone) are optimized as shown in Figures 5 and 6. Interestingly, it was found that

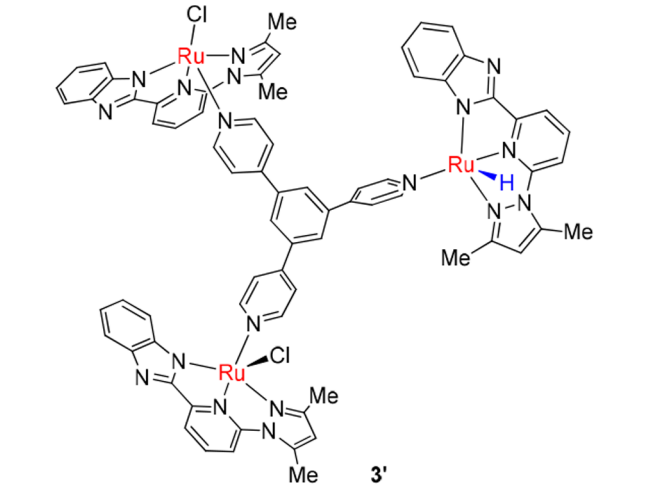

Figure 4. Optimized structure of complex **3′**.

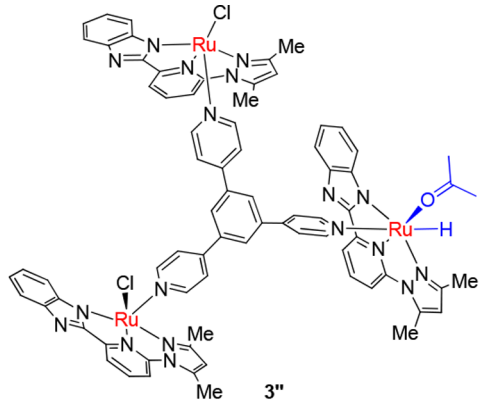

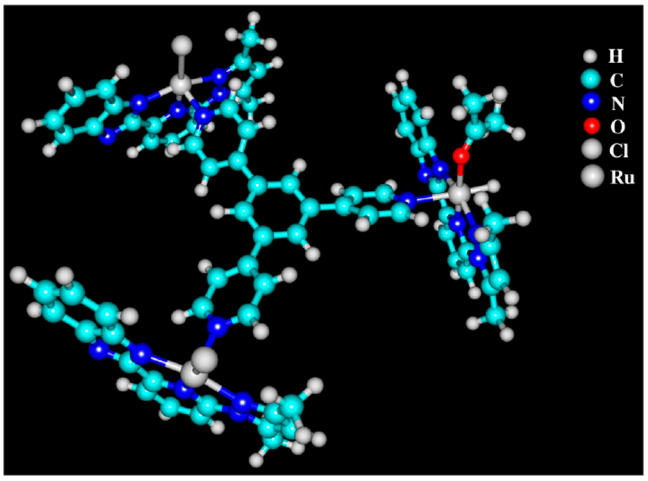

Figure 5. Optimized structure of complex **3″**.

ligand **2a** is positioned trans to the hydride in complex **3″**, and the NNN ligand of complex **1a** is situated trans to the coordinated ketone substrate (Figure 5). Similar structural features have also been found in the corresponding hydride species of complexes **9** and **10**, that is, Ru(II)−H complexes **9′** and **10′**.

Binding Energies. To understand the enhanced catalytic activity of the multinuclear Ru(II)−NNNN complex catalysts, their coordination and transfer hydrogenation behaviors were

DOI: 10.1021/acs.organomet.9b00669
Organometallics 2020, 39, 93−104

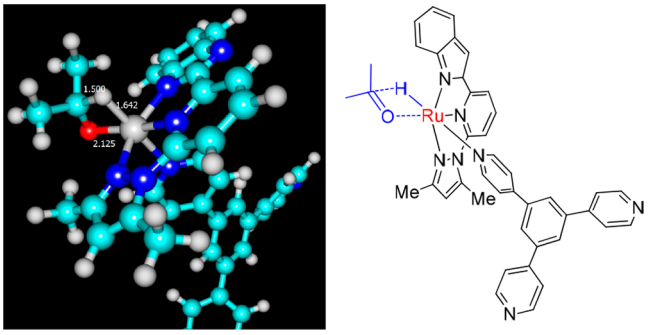

Figure 6. Optimized structure of the TH reaction transition state (bond lengths in Å).

modeled by means of Ru(II)−H complexes **9′**, **10′**, and **3′** as the model complex catalysts. The energies of the ketone substrate binding to the Ru(II)−H metal center of these three hydride complexes are 17.21, 17.53, and 18.26 kcal/mol, respectively. Upon binding of the ketone substrate, the energy barriers for the subsequent hydride transfer from the Ru(II)−H metal center to the ketone carbonyl are calculated to be 3.50, 3.72, and 3.90 kcal/mol (Figure 6). The energies for the PPh_3 ligand to bind the Ru(II)−H metal centers in **9′**, **10′**, and **3′** are 36.41, 36.85, and 36.49 kcal/mol, respectively, which are much greater than those for the ketone substrate to bind the same Ru(II)−H metal center. On the basis of the DFT calculations, it can be concluded that both dissociation of the PPh_3 ligand from the metal center and coordination of the ketone substrate to the metal center are crucial for the TH reaction to efficiently occur. The enhanced catalytic activity for complex catalyst **3′** mostly arises from the stronger capability of its Ru(II) metal center(s) to bind the ketone substrate, while the energy barrier for the transfer hydrogenation step is not sensitive to the environmental change around the metal centers in complexes **9′**, **10′**, and **3′**.

The energy difference for binding the ketone substrate between complexes **9′** and **3′** is ca. 1.1 kcal/mol. By means of Arrhenius equation with the assumption that the pre-exponential factor does not change, it is predicted that the TH reaction rate in the case of using complex **3′** as the model catalyst is about 6.4 times faster than that obtained by using the mononuclear Ru(II)−H complex **9′** as the catalyst at room temperature, which is within the experimental rate difference in our work as shown in Table 1.

To rationalize the stronger binding capability of multinuclear Ru(II)−NNNN complex **3′** for the ketone substrate, the structures and natural charges of the Ru(II)−H metal centers in complexes **9′**, **10′**, and **3′** were explored by variation of the chemical environment around the metal centers. It was found that all the Ru(II)−N, Ru(II)−O, and Ru(II)−H bond lengths are very close in these Ru−H complexes with a maximum deviation of less than 0.005 Å (see the Supporting Information for details). Ru(II)−hydride complexes **10′** and **3′** are almost structurally bestowed with the same Ru(II)−H metal center. This is also true for the natural charges on the Ru(II)−H metal centers with a maximum deviation of 0.005 e. These results have suggested that although the multinuclear Ru(II)−NNNN complex molecules are much bigger than the mononuclear one, the structural and electronic properties of the Ru(II) metal centers are actually very analogous. Next, the weak interaction of the ketone substrate coordinated to the Ru(II)−H metal center with the Ru(II)−Cl moieties in complex **3′** was considered. Such an interaction may also be contributed to the increase of the binding energy of the Ru(II)−H metal center and the ketone substrate. By means of IQA methods[27] utilizing the program ADF 2018[28] (M06−2x functional, tzp basis sets), the interaction energy between the ketone molecule coordinated to the Ru(II)−H metal center and the two Ru−Cl metal centers was calculated to be −0.75 kcal/mol, which results completely from the electrostatic interaction. This value is quite close to the binding energy difference between Ru(II)−H complexes **10′** and **3′** (−0.73 kcal/mol), implicating that the enhanced binding capability of complex **3′** arises from the weak electrostatic interaction between the ketone substrate and the Ru(II)−Cl fragments. The interaction between the coordinated ketone substrate and the two nearest CH_3 groups of the NNN ligand was also calculated with energy of 0.03 kcal/mol which could be ignored.

Proposed Mechanism. Thus, a plausible explanation is proposed to rationalize the enhanced catalytic activity of the multinuclear Ru(II)−NNNN complex catalysts. It is the weak electrostatic interaction between the coordinated ketone substrate and the metal centers of the Ru−Cl fragments, that is, the electrostatic attraction between the negatively charged oxygen of the ketone and the positively charged metal centers, which enhances the total binding strength of the Ru(II)−H metal center to the ketone substrate. As the spacer (linker) length in the oligopyridine ligand is extended, the electrostatic interaction between the coordinated ketone substrate and the Ru(II)−Cl fragments is then diminished, resulting in the observed decrease in the catalytic activity from **3** to **4** and from **6** to **7**, respectively, as shown in Tables 1 and 2 as well as Figures 2 and 3.

■ CONCLUSIONS

In summary, multinuclear ruthenium(II)−NNNN complexes have been constructed by assembly of a coordinatively unsaturated 16-electron mononuclear pincer-type Ru(II)−NNN complex and oligopyridine ligands. 1,3,5-Tri(pyridin-4-yl)-benzene-based triruthenium(II)−NNNN pincer complex has exhibited exceptionally high catalytic activity for the transfer hydrogenation of ketones at a very low loading. The enhanced catalytic activities of these multinuclear Ru(II)−NNNN complexes for the transfer hydrogenation of ketones have been rationalized by DFT calculations. The present assembly strategy provides a concise route to highly active transition metal complex catalysts.

■ EXPERIMENTAL SECTION

General Considerations. ^1H and $^{13}C\{^1H\}$ NMR spectra were recorded on a Bruker DRX-400 spectrometer and all chemical shift values refer to δ of TMS = 0.00 ppm, $CDCl_3$ ($\delta(^1H)$, 7.26 ppm; $\delta(^{13}C)$, 77.16 ppm), and DMSO-d_6 ($\delta(^1H)$, 2.50 ppm; $\delta(^{13}C)$, 39.52 ppm). Elemental analysis was achieved by the Analysis Center, Dalian University of Technology and Dalian Institute of Chemical Physics, Chinese Academy of Sciences. Matrix-assisted laser desorption/ionization time of flight mass spectra were recorded on a MALDI-TOF/TOF 5800 spectrometer. All the chemical reagents were purchased from commercial sources and used as received unless otherwise indicated.

Typical Procedures for the Synthesis of Complexes 3, 4, 6, 7, and 9. *Synthesis of Complex 3.* Under a nitrogen atmosphere, a mixture of complex **1a** (68.6 mg, 0.1 mmol) and ligand **2a** (10.3 mg, 0.03 mmol) in 3 mL of CH_2Cl_2/CH_3OH (v/v, 5/1) was stirred at 25 °C for 5 h. All the volatiles were removed under reduced pressure, and

DOI: 10.1021/acs.organomet.9b00669
Organometallics 2020, 39, 93−104

the resultant residue was subjected to purification by recrystallization in CH_2Cl_2/*n*-hexane (v/v, 1/3) at ambient temperature, affording complex **3** as a red solid (74 mg, 94%).

Synthesis of complex ***6***. Under a nitrogen atmosphere, a mixture of complex **1a** (68.6 mg, 0.1 mmol) and ligand **5a** (16.7 mg, 0.017 mmol) in 3 mL of CH_2Cl_2/CH_3OH (v/v, 5/1) was stirred at 25 °C for 5 h. All the volatiles were removed under reduced pressure and the resultant residue was subjected to purification by recrystallization in CH_2Cl_2/*n*-hexane (v/v, 1/3) at ambient temperature, affording complex **6** as a red solid (78 mg, 92%).

Synthesis of complex ***9***. Under a nitrogen atmosphere, complex **1a** (68.6 mg, 0.1 mmol) and ligand **8** (15.5 mg, 0.1 mmol) in 3 mL of CH_2Cl_2/CH_3OH (v/v, 5/1) was stirred at 25 °C for 5 h. All the volatiles were removed under reduced pressure, and the resultant residue was subjected to purification by recrystallization in CH_2Cl_2/*n*-hexane (v/v, 1/3) at ambient temperature to afford complex **9** as a dark red solid (80 mg, 92%).

Typical Procedure for the Transfer Hydrogenation Reaction of Ketones. The catalyst solution was prepared by dissolving complex **3** (9.4 mg, 0.004 mmol) in 2-propanol (60 mL). Under a nitrogen atmosphere, a mixture of a ketone (2.0 mmol), 7.5 mL of the catalyst solution (0.0005 mmol), and 2-propanol (12.1 mL) was stirred at 82 °C for 10 min. Then, 0.2 mL of *i*PrOK solution (0.01 mmol, 0.05 M) in 2-propanol was introduced to initiate the reaction. At the stated time, 0.1 mL of the reaction mixture was sampled and immediately diluted with 0.5 mL of 2-propanol precooled at 0 °C for GC analysis. After the reaction was complete, the reaction mixture was condensed under reduced pressure and subjected to purification by flash silica gel column chromatography to afford the corresponding alcohol product which was identified by comparison with the authentic sample through NMR and GC analyses.

Complex ***3***. 74 mg, 94%, red solid, mp > 300 °C dec. ^{1}H NMR (400 MHz, DMSO-d_6, 23 °C) δ 8.71 (d, J = 5.9 Hz, 6 H), 8.27 (s, 3 H), 8.08 (d, J = 8.0 Hz, 3 H), 8.00 (d, J = 6.0 Hz, 6 H), 7.62 (t, J = 8.1 Hz, 3 H), 7.56 (d, J = 7.7 Hz, 3 H), 7.43 and 7.31 (d each, J = 8.0 and 8.1 Hz, 3:3 H), 7.19−7.24 (m, 27 H), 7.05−7.11 (m, 3:18 H,), 6.98 (t, J = 7.5 Hz, 3 H), 6.38 (s, 3 H), 2.69 (s, 9 H), 2.52 (s, 9 H), 2.52. ^{13}C{^{1}H} NMR (100 MHz, DMSO-d_6, 23 °C) δ 156.9, 154.4, 151.5, 150.1, 146.3, 145.5, 144.7, 139.2, 131.6 (d, J = 62.0 Hz, *i*-C of PPh_3) and 129.0 (Cq each), 150.2, 136.0, 132.9 (d, J = 15.7 Hz, *o*-C of PPh_3), 129.3, 127.7 (d, J = 13.9 Hz, *m*-C of PPh_3), 126.2, 121.8, 121.1, 120.5, 117.9, 117.4, 116.5, 112.6, 108.4, 14.4, 14.2. ^{31}P{^{1}H} NMR (162 MHz, DMSO-d_6, 23 °C) δ 33.5. IR (KBr pellets, cm^{-1}): ν 3430, 3051, 2955, 2920, 2853, 2568, 2373, 2344, 1813, 1774, 1735, 1719, 1551, 1500, 1478, 1408, 1355, 1280, 1218, 1186, 1157, 1117, 1070, 1048, 1033, 1000, 983, 913, 892, 843, 818, 720, 669, 658, 620, 573, 528, 502, 468, 436. Anal. Calcd for $C_{126}H_{102}Cl_3N_{18}P_3Ru_3$: C, 63.83; H, 4.34; N, 10.63. Found: C, 63.73; H, 4.38; N, 10.52. MALDI-TOF MS (m/z) Calcd for $[C_{35}H_{29}ClN_5PRu + H]^+$: 688.0971. Found: 688.0292. MALDI-TOF MS (m/z) Calcd for $[C_{21}H_{15}N_3 + H]^+$: 310.1339. Found: 310.1230.

Complex ***4***. 77 mg, 91%, red solid, mp > 300 °C dec. ^{1}H NMR (400 MHz, DMSO-d_6, 23 °C) δ 8.69 (d, J = 5.5 Hz, 6 H), 8.06−8.10 (m, 3:3:6 H), 7.98 (d, J = 8.1 Hz, 6 H), 7.81 (d, J = 5.4 Hz, 6 H), 7.62 (t, J = 8.0 Hz, 3 H), 7.55 (d, J = 7.6 Hz, 3 H), 7.44 and 7.31 (d each, J = 8.0 and 8.1 Hz, 3:3 H), 7.19−7.24 (m, 27 H), 7.04−7.11 (m, 3:18 H), 6.97 (t, J = 7.4 Hz, 3 H), 6.37 (s, 3 H), 2.69 (s, 9 H), 2.52 (s, 9 H). ^{13}C{^{1}H} NMR (100 MHz, DMSO-d_6, 23 °C) δ 158.8, 156.9, 154.4, 151.5, 151.4, 146.4, 145.5, 144.7, 141.0, 140.8, 131.6 (d, J = 62.0 Hz, *i*-C of PPh_3) and 129.0 (Cq each), 150.3, 136.5, 136.0, 132.9 (d, J = 16.4 Hz, *o*-C of PPh_3), 129.4, 128.1, 127.7 (d, J = 14.6 Hz, *m*-C of PPh_3), 127.4, 124.8, 121.1, 120.5, 117.9, 117.4, 116.5, 112.6, 108.4, 14.4, 14.2. ^{31}P{^{1}H} NMR (162 MHz, DMSO-d_6, 23 °C) δ 33.5. IR (KBr pellets, cm^{-1}): ν 3050, 2960, 2918, 2854, 2755, 2677, 1956, 1815, 1720, 1626, 1573, 1551, 1500, 1478, 1435, 1409, 1395, 1356, 1301, 1270, 1229, 1186, 1157, 1141, 1094, 1069, 1049, 1021, 1005, 983, 930, 889, 845, 791, 659, 619, 590, 515, 500, 462, 436, 410. Anal. Calcd for $C_{144}H_{114}Cl_3N_{18}P_3Ru_3$: C, 66.54; H, 4.42; N, 9.70. Found: C, 66.41; H, 4.47; N, 9.61. MALDI-TOF MS (m/z) Calcd for $[C_{35}H_{29}ClN_5PRu + H]^+$: 688.0971. Found: 687.9938. MALDI-TOF MS (m/z) Calcd for $[C_{39}H_{27}N_3 + H]^+$: 538.2278. Found: 538.1482.

Complex ***6***. 78 mg, 92%, red solid, mp > 300 °C dec. ^{1}H NMR (400 MHz, DMSO-d_6, 23 °C) δ 8.42 and 8.08 (d each, J = 5.1 and 8.1 Hz, 12:6 H), 7.55−7.64 (m, 6:6:12 H), 7.43 (m, 12:12 H), 7.31 (d, J = 8.2 Hz, 6 H), 7.16−7.24 (m, 54 H), 7.04−7.11 (m, 36:6:6 H), 6.98 (t, J = 7.4 Hz, 6 H), 6.37 (s, 6 H), 2.69 (s, 18 H), 2.53 (s, 18 H). ^{13}C{^{1}H} NMR (100 MHz, DMSO-d_6, 23 °C) δ 160.1, 156.7, 155.3, 151.5, 150.1, 147.0, 146.1, 139.7, 135.8, 131.5, 131.4 and 128.8 (Cq each), 132.9 (d, J = 16.2 Hz, *o*-C of PPh_3), 131.8 (d, J = 74.7 Hz, *i*-C PPh_3), 129.2 (s, *p*-C of PPh_3), 127.6 (d, J = 14.4 Hz, *m*-C of PPh_3), 144.5, 128.7, 127.5, 124.9, 120.5, 120.4, 119.5, 118.7, 117.1, 116.1, 112.4, 107.9, 14.4, 14.1. ^{31}P{^{1}H} NMR (162 MHz, DMSO-d_6, 23 °C) δ 33.5. IR (KBr pellets, cm^{-1}): ν 3435, 3050, 2954, 2918, 2855, 2584, 2347, 1911, 1813, 1775, 1606, 1573, 1550, 1499, 1478, 1459, 1435, 1409, 1354, 1325, 1280, 1219, 1186, 1157, 1142, 1093, 1048, 1033, 1001, 982, 930, 844, 820, 789, 746, 619, 577, 528, 514, 499, 465, 436. Anal. Calcd for $C_{282}H_{222}Cl_6N_{36}P_6Ru_6$: C, 66.15; H, 4.37; N, 9.85. Found: C, 66.07; H, 4.34; N, 9.82. MALDI-TOF MS (m/z) Calcd for $[C_{35}H_{29}ClN_5PRu + H]^+$: 688.0971. Found: 688.0164. MALDI-TOF MS (m/z) Calcd for $[C_{72}H_{48}N_6 + H]^+$: 997.4013. Found: 997.2916.

Complex ***7***. 80 mg, 91%, red solid, mp > 300 °C dec. ^{1}H NMR (400 MHz, DMSO-d_6, 23 °C) δ 8.57 (d, J = 5.7 Hz, 12 H), 8.16 and 7.70 (d and m, J = 8.2 Hz,6:12 H), 7.38−7.51 (m, 24 H), 7.19−7.24 (m, 54:6:12 H), 7.02−7.12 (m, 36:6:12 H), 6.39 (s, 6 H), 2.70 (s, 18 H), 2.54 (s, 18 H). ^{13}C{^{1}H} NMR (100 MHz, DMSO-d_6, 23 °C) δ 157.0, 153.7, 151.6, 151.4, 145.0, 144.9, 140.6, 139.4, 131.5 (d, J = 62.2 Hz, *i*-C of PPh_3), 130.4, 130.0 and 125.7 (Cq each), 149.9, 136.1, 132.8 (d, J = 16.2 Hz, *o*-C of PPh_3), 129.4, 127.7 (d, J = 14.6 Hz, *m*-C of PPh_3), 125.3, 121.5, 118.8, 117.7, 116.8, 112.6, 121.1, 117.3, 108.7, 93.3 and 87.0 (C≡C, Cq each), 14.4, 14.1. ^{31}P{^{1}H} NMR (162 MHz, DMSO-d_6, 23 °C) δ 33.0. IR (KBr pellets, cm^{-1}): ν 3441, 2957, 2919, 2584, 2217, 1955, 1774, 1604, 1550, 1501, 1478, 1435, 1409, 1354, 1280, 1234, 1214, 1185, 1157, 1142, 1048, 1032, 1018, 1000, 985, 913, 824, 789, 772, 655, 640, 620, 578, 514, 499, 464, 436. Anal. Calcd for $C_{294}H_{222}Cl_6N_{36}P_6Ru_6$: C, 67.08; H, 4.25; N, 9.58. Found: C, 67.15; H, 4.22; N, 9.49. MALDI-TOF MS (m/z) Calcd for $[C_{35}H_{29}ClN_5PRu + H]^+$: 688.0971. Found: 687.9626. MALDI-TOF MS (m/z) Calcd for $[C_{84}H_{48}N_6 + H]^+$: 1141.4012. Found: 1141.2973.

Complex ***9***. 80 mg, 92%, red solid, mp > 300 °C dec. ^{1}H NMR (400 MHz, DMSO-d_6, 23 °C) δ 8.64 (dd, J = 4.5, 1.7 Hz, 2 H), 8.07 (d, J = 8.1 Hz, 1 H), 7.81 (dd, J = 9.5, 2.6 Hz, 2 H), 7.71 (dd, J = 4.5, 1.7 Hz, 2 H), 7.62 (t, J = 8.0 Hz, 1 H), 7.57−7.45 (m, 4 H), 7.43 (d, J = 8.0 Hz, 1 H), 7.31 (d, J = 7.5 Hz, 1 H), 7.25−7.18 (m, 9 H), 7.08 (dtd, J = 10.0, 8.3, 1.5 Hz, 7 H), 6.93−6.99 (m, 1 H), 6.37 (s, 1 H), 2.69 (s, 3 H), 2.52 (s, 3 H). ^{13}C{^{1}H} NMR (100 MHz, DMSO-d_6, 23 °C) δ 160.1, 156.7, 155.3, 151.7, 151.5, 147.0, 146.1, 144.5 and 150.2 (Cq each), 137.1, 135.8, 132.9 (d, J = 16.4 Hz, *o*-C of PPh_3), 131.8 (d, J = 61.6 Hz, *i*-C of PPh_3), 129.2, 129.2, 129.1, 127.6 (d, J = 14.4 Hz, *m*-C of PPh_3), 126.8, 121.2, 120.5, 119.5, 118.7, 117.1, 116.1, 112.4, 107.9, 14.4, 14.1. ^{31}P{^{1}H} NMR (162 MHz, DMSO-d_6, 23 °C) 33.5. IR (KBr pellets, cm^{-1}): ν 3439, 3052, 3004, 2958, 2921, 2869, 1607, 1574, 1550, 1500, 1481, 1459, 1436, 1410, 1396, 1354, 1326, 1280, 1219, 1186, 1157, 1141, 1094, 1070, 1048, 1034, 1011, 1002, 982, 841, 834, 788, 767, 698, 659, 623, 578, 562, 527, 515, 500, 462, 447, 437,427. Anal. Calcd for $C_{46}H_{38}ClN_6PRu$: C, 65.59; H, 4.55; N, 9.98. Found: C, 65.47; H, 4.60; N, 9.89.

■ ASSOCIATED CONTENT

Supporting Information

The Supporting Information is available free of charge at https://pubs.acs.org/doi/10.1021/acs.organomet.9b00669.

Experimental materials and procedures, analytical data and NMR spectra of compounds and complexes MALDI-TOF MS spectra of complexes, theoretical methods and results (PDF)

Cartesian coordinates (XYZ)

DOI: 10.1021/acs.organomet.9b00669
Organometallics 2020, 39, 93−104

AUTHOR INFORMATION

Corresponding Authors

*E-mail: zkyu@dicp.ac.cn (Z.K.Y.).
*E-mail: fanhj@dicp.ac.cn (H.J.F.).
*E-mail: ygzhou@dicp.ac.cn (Y.G.Z.).

ORCID

Tingting Liu: 0000-0002-0156-3054
Kaikai Wu: 0000-0003-1950-5343
Liandi Wang: 0000-0003-4996-3687
Hongjun Fan: 0000-0003-3406-6932
Yong-Gui Zhou: 0000-0002-3321-5521
Zhengkun Yu: 0000-0002-9908-0017

Notes

The authors declare no competing financial interest.

ACKNOWLEDGMENTS

We are grateful to the National Natural Science Foundation of China (21672209 and 21871253) and the strategic pilot science and technology project of the Chinese Academy of Sciences (XDB17010200) for support of this research.

REFERENCES

(1) (a) Gunanathan, C.; Milstein, D. Metal-Ligand Cooperation by Aromatization- Dearomatization: A New Paradigm in Bond Activation and "Green" Catalysis. *Acc. Chem. Res.* **2011**, *44*, 588−602. (b) Yamaguchi, R.; Ikeda, C.; Takahashi, Y.; Fujita, K. Homogeneous Catalytic System for Reversible Dehydrogenation-Hydrogenation Reactions of Nitrogen Heterocycles with Reversible Interconversion of Catalytic Species. *J. Am. Chem. Soc.* **2009**, *131*, 8410−8412.

(2) (a) Powers, I. G.; Uyeda, C. Metal-Metal Bonds in Catalysis. *ACS Catal.* **2017**, *7*, 936−958. (b) Buchwalter, P.; Rosé, J.; Braunstein, P. Multimetallic Catalysis Based on Heterometallic Complexes and Clusters. *Chem. Rev.* **2015**, *115*, 28−126. (c) Xu, Y. H.; Fischer, A.; Duan, L. L.; Tong, L. P.; Gabrielsson, E.; Akermark, B.; Sun, L. C. Chemical and Light-driven Oxidation of Water Catalyzed by an Efficient Dinuclear Ruthenium Complex. *Angew. Chem., Int. Ed.* **2010**, *49*, 8934−8937.

(3) (a) Wang, B.; Luo, G.; Nishiura, M.; Hu, S.; Shima, T.; Luo, Y.; Hou, Z. Dinitrogen Activation by Dihydrogen and a PNP-Ligated Titanium Complex. *J. Am. Chem. Soc.* **2017**, *139*, 1818−1821. (b) Ouyang, T.; Huang, H.-H.; Wang, J.-W.; Zhong, D.-C.; Lu, T.-B. A Dinuclear Cobalt Cryptate as a Homogeneous Photocatalyst for Highly Selective and Efficient Visible-Light Driven CO_2 Reduction to CO in CH_3CN/H_2O Solution. *Angew. Chem., Int. Ed.* **2017**, *56*, 738−743. (c) Veronelli, M.; Dechert, S.; Demeshko, S.; Meyer, F. 1,1′-Bis(pyrazol-3-yl)ferrocene: A Clip Ligand That Forms Supramolecular Aggregates and Prismatic Hexanuclear Coinage Metal Complexes. *Inorg. Chem.* **2015**, *54*, 6917−6927. (d) Lu, X.; Li, X.; Cao, Y.; Schultz, A.; Wang, J.-L.; Moorefield, C. N.; Wesdemiotis, C.; Cheng, S. Z. D.; Newkome, G. R. Self-Assembly of a Supramolecular, Three-Dimensional, Spoked, Bicycle-like Wheel. *Angew. Chem., Int. Ed.* **2013**, *52*, 7728−7731.

(4) (a) Vanicek, S.; Podewitz, M.; Stubbe, J.; Schulze, D.; Kopacka, H.; Wurst, K.; Meller, T.; Lippmann, P.; Haslinger, S.; Schottenberger, H.; et al. Highly Electrophilic, Catalytically Active and Redox-Responsive Cobaltoceniumyl and Ferrocenyl Triazolylidene Coinage Metal Complexes. *Chem. - Eur. J.* **2018**, *24*, 3742−3753. (b) Hicken, A.; White, A. J. P.; Crimmin, M. R. Selective Reduction of CO_2 to a Formate Equivalent with Heterobimetallic Gold–Copper Hydride Complexes. *Angew. Chem., Int. Ed.* **2017**, *56*, 15127−15130. (c) Jiang, X.-F.; Huang, H.; Chai, Y.-F.; Lohr, T. L.; Yu, S.-Y.; Lai, W.; Pan, Y.-J.; Delferro, M.; Marks, T. J. Hydrolytic Cleavage of Both CS_2 Carbon−Sulfur Bonds by Multinuclear Pd(II) Complexes at Room Temperature. *Nat. Chem.* **2017**, *9*, 188−193. (d) Zhu, B.; Guan, W.; Yan, L.-K.; Su, Z.-M. Two-State Reactivity Mechanism of Benzene C−C Activation by Trinuclear Titanium Hydride. *J. Am. Chem. Soc.* **2016**, *138*, 11069−11072.

(5) (a) Gu, X.; Li, X.; Wu, S.; Shi, J.; Jiang, G.; Jiang, G.; Tian, S. A Sensitive Hydrazine Hydrate Sensor Based on A Mercaptomethyl-terminated Trinuclear Ni(II)-Complex Modified Gold Electrode. *RSC Adv.* **2016**, *6*, 8070−8078. (b) Mognon, L.; Mandal, S.; Castillo, C. E.; Fortage, J.; Molton, F.; Aromí, G.; Benet-Buchhlolz, J.; Collomb, M.-N.; Llobet, A. Synthesis, Structure, Spectroscopy and Reactivity of New Heterotrinuclear Water Oxidation Catalysts. *Chem. Sci.* **2016**, *7*, 3304−3312. (c) Liu, R.; von Malotki, C.; Arnold, L.; Koshino, N.; Higashimura, H.; Baumgarten, M.; Müllen, K. Triangular Trinuclear Metal-N_4 Complexes with High Electrocatalytic Activity for Oxygen Reduction. *J. Am. Chem. Soc.* **2011**, *133*, 10372−10375.

(6) (a) Yamazaki, Y.; Umemoto, A.; Ishitani, O. Photochemical Hydrogenation of π-Conjugated Bridging Ligands in Photofunctional Multinuclear Complexes. *Inorg. Chem.* **2016**, *55*, 11110−11124. (b) Sahara, G.; Abe, R.; Higashi, M.; Morikawa, T.; Maeda, K.; Ueda, Y.; Ishitani, O. Photoelectrochemical CO_2 Reduction Using a Ru(II)−Re(I) Multinuclear Metal Complex on A P-type Semiconducting NiO Electrode. *Chem. Commun.* **2015**, *51*, 10722−10725.

(7) (a) Andruh, M. Heterotrimetallic Complexes in Molecular Magnetism. *Chem. Commun.* **2018**, *54*, 3559−3577. (b) Dul, M.-C.; Pardo, E.; Lescouëzec, R.; Journaux, Y.; Ferrando-Soria, J.; Ruiz-García, R.; Cano, J.; Julve, M.; Lloret, F.; Cangussu, D.; Pereira, C. L. M.; Stumpf, H. O.; Pasán, J.; Ruiz-Pérez, C. Supramolecular Coordination Chemistry of Aromatic Polyoxalamide Ligands: A Metallosupramolecular Approach Toward Functional Magnetic Materials. *Coord. Chem. Rev.* **2010**, *254*, 2281−2296.

(8) (a) Metherell, A. J.; Ward, M. D. Stepwise Synthesis of Mixed-Metal Assemblies Using Pre-formed Ru(II) 'Complex Ligands' as Building Blocks. *RSC Adv.* **2016**, *6*, 10750−10762. (b) Zhang, Y.-Y.; Zhang, L.; Lin, Y.-J.; Jin, G.-X. Mixed-Metal Coordination Cages Constructed with Pyridyl-Functionalized β-Diketonate Metalloligands: Syntheses, Structures and Host−Guest Properties. *Chem. - Eur. J.* **2015**, *21*, 14893−14900.

(9) (a) Floris, B.; Donzello, M. P.; Ercolani, C.; Viola, E. The Chameleon-like Coordinating Ability of 2,3-Di(pyridyl)pyrazine-type Ligands. *Coord. Chem. Rev.* **2017**, *347*, 115−140. (b) Sinha, N.; Hahn, F. E. Metallosupramolecular Architectures Obtained from Poly-N-heterocyclic Carbene Ligands. *Acc. Chem. Res.* **2017**, *50*, 2167−2184. (c) McWilliams, S. F.; Holland, P. L. Dinitrogen Binding and Cleavage by Multinuclear Iron Complexes. *Acc. Chem. Res.* **2015**, *48*, 2059−2065.

(10) (a) Sepehrpour, H.; Saha, M. L.; Stang, P. J. Fe-Pt Twisted Heterometallic Bicyclic Supramolecules via Multicomponent Self-Assembly. *J. Am. Chem. Soc.* **2017**, *139*, 2553−2556. (b) Cook, T. R.; Stang, P. J. Recent Developments in the Preparation and Chemistry of Metallacycles and Metallacages via Coordination. *Chem. Rev.* **2015**, *115*, 7001−7045. (c) Yan, X.; Wang, H.; Hauke, C. E.; Cook, T. R.; Wang, M.; Saha, M. L.; Zhou, Z.; Zhang, M.; Li, X.; Huang, F.; Stang, P. J. A Suite of Tetraphenylethylene-Based Discrete Organoplatinum(II) Metallacycles: Controllable Structure and Stoichiometry, Aggregation-Induced Emission, and Nitroaromatics Sensing. *J. Am. Chem. Soc.* **2015**, *137*, 15276−15286.

(11) (a) Richert, S.; Limburg, B.; Anderson, H. L.; Timmel, C. R. On the Influence of the Bridge on Triplet State Delocalization in Linear Porphyrin Oligomers. *J. Am. Chem. Soc.* **2017**, *139*, 12003−12008. (b) Favereau, L.; Cnossen, A.; Kelber, J. B.; Gong, J. Q.; Oetterli, R.; Cremers, J.; Herz, L. M.; Anderson, H. L. Six-Coordinate Zinc Porphyrins for Template-Directed Synthesis of Spiro-Fused Nanorings. *J. Am. Chem. Soc.* **2015**, *137*, 14256−14259.

(12) (a) Shiga, T.; Newton, G. N.; Oshio, H. Pre-programmed Self-Assembly of Polynuclear Clusters. *Dalton Trans.* **2018**, *47*, 7384−7394. (b) Dutta, I.; Sarbajna, A.; Pandey, P.; Rahaman, S. M. W.; Singh, K.; Bera, J. K. Acceptorless Dehydrogenation of Alcohols on a Diruthenium(II, II) Platform. *Organometallics* **2016**, *35*, 1505−1513. (c) Saha, B.; Rahaman, S. M. W.; Daw, P.; Sengupta, G.; Bera, J. K. Metal−Ligand Cooperation on a Diruthenium Platform: Selective

DOI: 10.1021/acs.organomet.9b00669
Organometallics 2020, 39, 93−104

Imine Formation through Acceptorless Dehydrogenative Coupling of Alcohols with Amines. *Chem. - Eur. J.* **2014**, *20*, 6542−6551. (d) Debata, N. B.; Tripathy, D.; Chand, D. K. Self-assembled Coordination Complexes from Various Palladium(II) Components and Bidentate or Polydentate Ligands. *Coord. Chem. Rev.* **2012**, *256*, 1831−1945. (e) Chakrabarty, R.; Mukherjee, P. S.; Stang, P. J. Supramolecular Coordination: Self-Assembly of Finite Two- and Three-Dimensional Ensembles. *Chem. Rev.* **2011**, *111*, 6810−6918.

(13) (a) Bloch, W. M.; Clever, G. H. Integrative Self-Sorting of Coordination Cages Based on 'Naked' Metal Ions. *Chem. Commun.* **2017**, *53*, 8506−8516. (b) Clever, G. H.; Punt, P. Cation−Anion Arrangement Patterns in Self-Assembled Pd_2L_4 and Pd_4L_8 Coordination Cages. *Acc. Chem. Res.* **2017**, *50*, 2233−2243. (c) Cook, T. R.; Zheng, Y.-R.; Stang, P. J. Metal−Organic Frameworks and Self-Assembled Supramolecular Coordination Complexes: Comparing and Contrasting the Design, Synthesis, and Functionality of Metal−Organic Materials. *Chem. Rev.* **2013**, *113*, 734−777.

(14) Wang, D.; Astruc, D. The Golden Age of Transfer Hydrogenation. *Chem. Rev.* **2015**, *115*, 6621−6686.

(15) (a) Noyori, R. Facts are the enemy of truth-reflections on serendipitous discovery and unforeseen developments in asymmetric catalysis. *Angew. Chem., Int. Ed.* **2013**, *52*, 79−92. (b) Ohkuma, T.; Utsumi, N.; Tsutsumi, K.; Murata, K.; Sandoval, C.; Noyori, R. The Hydrogenation/transfer hydrogenation network: asymmetric hydrogenation of ketones with chiral η^6-arene/N-tosylethylenediamine-ruthenium catalysts. *J. Am. Chem. Soc.* **2006**, *128*, 8724−8725. (c) Kitamura, M.; Noyori, R. In *Ruthenium in Organic Synthesis*; Murahashi, S.-I., Ed.; Wiley-VCH: Weinheim, 2004; pp 3−52. (d) Noyori, R.; Ohkuma, T. Asymmetric Catalysis by Architectural and Functional Molecular Engineering: Practical Chemo and Stereoselective. *Angew. Chem., Int. Ed.* **2001**, *40*, 40−73. (e) Yamakawa, M.; Yamada, I.; Noyori, R. CH/π attraction: the origin of enantioselectivity in transfer hydrogenation of aromatic carbonyl compounds catalyzed by chiral η^6-arene-ruthenium(II) complexes. *Angew. Chem., Int. Ed.* **2001**, *40*, 2818−2821.

(16) Zimbron, J. M.; Dauphinais, M.; Charette, A. B. Noyori−Ikariya Catalyst Supported on Tetraarylphosphonium Salt for Asymmetric Transfer Hydrogenation in Water. *Green Chem.* **2015**, *17*, 3255−3259.

(17) (a) Zuo, W. W.; Morris, R. H. Synthesis and Use of An Asymmetric Transfer Hydrogenation Catalyst Based on Iron(II) for the Synthesis of Enantioenriched Alcohols and Amines. *Nat. Protoc.* **2015**, *10*, 241−257. (b) Zuo, W. W.; Lough, A. J.; Li, Y. F.; Morris, R. H. Amine(imine)diphosphine Iron Catalysts for Asymmetric Transfer Hydrogenation of Ketones and Imines. *Science* **2013**, *342*, 1080−1083.

(18) Chelucci, G.; Baldino, S.; Baratta, W. Recent Advances in Osmium-Catalyzed Hydrogenation and Dehydrogenation Reactions. *Acc. Chem. Res.* **2015**, *48*, 363−379.

(19) (a) Chai, H. N.; Liu, T. T.; Yu, Z. K. NHTs Effect on the Enantioselectivity of Ru(II) Complex Catalysts Bearing a Chiral Bis(NHTs)-Substituted Imidazolyl-Oxazolinyl Pyridine Ligand for Asymmetric Transfer Hydrogenation of Ketones. *Organometallics* **2017**, *36*, 4136−4144. (b) Chai, H. N.; Liu, T. T.; Wang, Q. F.; Yu, Z. K. Substituent Effect on the Catalytic Activity of Ruthenium(II) Complexes Bearing a Pyridyl-Supported Pyrazolyl-Imidazolyl Ligand for Transfer Hydrogenation of Ketones. *Organometallics* **2015**, *34*, 5278−5284. (c) Du, W. M.; Wang, L. D.; Wu, P.; Yu, Z. K. A Versatile Ruthenium(II)−NNC Complex Catalyst for Transfer Hydrogenation of Ketones and Oppenauer-Type Oxidation of Alcohols. *Chem. - Eur. J.* **2012**, *18*, 11550−11554. (d) Ye, W. J.; Zhao, M.; Du, W. M.; Jiang, Q. B.; Wu, K. K.; Wu, P.; Yu, Z. K. Highly Active Ruthenium(II) Complex Catalysts Bearing an Unsymmetrical NNN Ligand in the (Asymmetric) Transfer Hydrogenation of Ketones. *Chem. - Eur. J.* **2011**, *17*, 4737−4741. (e) Zeng, F. L.; Yu, Z. K. Construction of Highly Active Ruthenium(II)-NNN Complex Catalysts Bearing a Pyridyl-Supported Pyrazolyl-Imidazolyl Ligand for Transfer Hydrogenation of Ketones. *Organometallics* **2009**, *28*, 1855−1862.

(20) (a) Chai, H. N.; Liu, T. T.; Zheng, D. Y.; Yu, Z. K Cooperative N-H and CH_2 Skeleton Effects on the Catalytic Activities of Bimetallic Ru(II)-NNN Complexes: Experimental and Theoretical Study. *Organometallics* **2017**, *36*, 4268−4277. (b) Wang, Q. F.; Chai, H. N.; Yu, Z. K. Dimeric Ruthenium(II)-NNN Complex Catalysts Bearing a Pyrazolyl-Pyridylamino-Pyridine Ligand for Transfer Hydrogenation of Ketones and Acceptorless Dehydro-genation of Alcohols. *Organometallics* **2017**, *36*, 3638−3644. (c) Liu, T. T.; Chai, H. N.; Wang, L. D.; Yu, Z. K. Exceptionally Active Assembled Dinuclear Ruthenium(II)-NNN Complex Catalysts for Transfer Hydrogenation of Ketones. *Organometallics* **2017**, *36*, 2914−2921. (d) Chai, H. N.; Wang, Q. F.; Liu, T. T.; Yu, Z. K. Diruthenium(II)−NNN Pincer Complex Catalysts for Transfer Hydrogenation of Ketones. *Dalton Trans.* **2016**, *45*, 17843−17849.

(21) (a) Schmittel, M.; He, B.; Mal, P. Supramolecular Multicomponent Self-Assembly of Shape-Adaptive Nanoprisms: Wrapping up C_{60} with Three Porphyrin Units. *Org. Lett.* **2008**, *10*, 2513−2516. (b) Fujita, M.; Oka, H.; Ogura, K. Palladium(0)/LiCl Promoted Cross-Coupling Reaction of (4-Pyridyl)stannanes and Aromatic Bromides: Easy Access to Poly(4-pyridyl)-Substituted Aromatics. *Tetrahedron Lett.* **1995**, *36*, 5247−5250. (c) Hoffmann, M.; Kärnbratt, J.; Chang, M.-H.; Herz, L. M.; Albinsson, B.; Anderson, H. L. Enhanced π Conjugation around a Porphyrin[6] Nanoring. *Angew. Chem., Int. Ed.* **2008**, *47*, 4993−4996. (d) Zhu, B.; Chen, H.; Lin, W.; Ye, Y.; Wu, J.; Li, S. Template-Directed Synthesis of Flexible Porphyrin Nanocage and Nanorings via One-Step Olefin Metathesis. *J. Am. Chem. Soc.* **2014**, *136*, 15126−15129.

(22) (a) Hilger, A.; Gisselbrecht, J.-P.; Tykwinski, R. R.; Boudon, C.; Schreiber, M.; Martin, R. E.; Lüthi, H. P.; Gross, M.; Diederich, F. Electronic Characteristics of Arylated Tetraethynylethenes: A Cooperative Computational and Electrochemical Investigation. *J. Am. Chem. Soc.* **1997**, *119*, 2069−2078. (b) Mccleverty, J. A.; Ward, M. D. The Role of Bridging Ligands in Controlling Electronic and Magnetic Properties in Polynuclear Complexes. *Acc. Chem. Res.* **1998**, *31*, 842−851.

(23) (a) Baratta, W.; Ballico, M.; Del Zotto, A.; Herdtweck, E.; Magnolia, S.; Peloso, R.; Siega, K.; Toniutti, M.; Zangrando, E.; Rigo, P. Pincer CNN Ruthenium(II) Complexes with Oxygen-Containing Ligands (O_2CR, OAr, OR, $OSiR_3$, O_3SCF_3): Synthesis, Structure, and Catalytic Activity in Fast Transfer Hydrogenation. *Organometallics* **2009**, *28*, 4421−4430. (b) Chelucci, G.; Baldino, S.; Baratta, W. Ruthenium and Osmium Complexes Containing 2-(Aminomethyl)-pyridine (Ampy)-based Ligands in Catalysis. *Coord. Chem. Rev.* **2015**, *300*, 29−85. (c) Blackmond, D. G. Reaction Progress Kinetic Analysis: A Powerful Methodology for Mechanistic Studies of Complex Catalytic Reactions. *Angew. Chem., Int. Ed.* **2005**, *44*, 4302−4320.

(24) (a) Tseng, K.-N. T.; Kampf, J. W.; Szymczak, N. K. Mechanism of N, N, N-Amide Ruthenium(II) Hydride Mediated Acceptorless Alcohol Dehydrogenation: Inner-Sphere β-H Elimination versus Outer-Sphere Bifunctional Metal-Ligand Cooperativity. *ACS Catal.* **2015**, *5*, 5468−5485. (b) Matsubara, Y.; Fujita, E.; Doherty, M. D.; Muckerman, J. T.; Creutz, C. Thermodynamic and Kinetic Hydricity of Ruthenium(II) Hydride Complexes. *J. Am. Chem. Soc.* **2012**, *134*, 15743−15757.

(25) Zhao, Y.; Truhlar, D. G. A New Local Density Functional for Main-group Thermochemistry, Transition Metal Bonding, Thermochemical Kinetics, and Noncovalent Interactions. *J. Chem. Phys.* **2006**, *125*, 194101.

(26) Frisch, M. J.; Trucks, G. W.; Schlegel, H. B.; Scuseria, G. E.; Robb, M. A.; Cheeseman, J. R.; Scalmani, G.; Barone, V.; Petersson, G. A.; Nakatsuji, H.; Li, X.; Caricato, M.; Marenich, A. V.; Bloino, J.; Janesko, B. G.; Gomperts, R.; Mennucci, B.; Hratchian, H. P.; Ortiz, J. V.; Izmaylov, A. F.; Sonnenberg, J. L.; Williams-Young, D.; Ding, F.; Lipparini, F.; Egidi, F.; Goings, J.; Peng, B.; Petrone, A.; Henderson, T.; Ranasinghe, D.; Zakrzewski, V. G.; Gao, J.; Rega, N.; Zheng, G.; Liang, W.; Hada, M.; Ehara, M.; Toyota, K.; Fukuda, R.; Hasegawa, J.; Ishida, M.; Nakajima, T.; Honda, Y.; Kitao, O.; Nakai, H.; Vreven, T.; Throssell, K.; Montgomery, J. A., Jr.; Peralta, J. E.; Ogliaro, F.;

DOI: 10.1021/acs.organomet.9b00669
Organometallics 2020, 39, 93−104

Bearpark, M.; Heyd, J. J.; Brothers, E. N.; Kudin, K. N.; Staroverov, V. N.; Kobayashi, R.; Normand, J.; Raghavachari, K.; Rendell, A.; Burant, J. C.; Iyengar, S. S.; Tomasi, J.; Cossi, M.; Millam, J. M.; Klene, M.; Adamo, C.; Cammi, R.; Ochterski, J. W.; Martin, R. L.; Morokuma, K.; Farkas, O.; Foresman, J. B.; Fox, D. J. *Gaussian 16*, revision A.03; Gaussian, Inc.: Wallingford CT, 2016.

(27) Blanco, I.; Pendás, A. M.; Francisco, E. Interacting Quantum Atoms: A Correlated Energy Decomposition Scheme Based on the Quantum Theory of Atoms in Molecules. *J. Chem. Theory Comput.* **2005**, *1*, 1096−1109.

(28) *ADF 2018*; SCM, Theoretical Chemistry, Vrije Universiteit, Amsterdam, The Netherlands, 2018.

DOI: 10.1021/acs.organomet.9b00669
Organometallics 2020, 39, 93−104